

Low-Loss Optomechanical Oscillator for Quantum-Optics Experiments

A. Borrielli,^{1,2} A. Pontin,^{3,4} F. S. Cataliotti,^{3,4,5} L. Marconi,³ F. Marin,^{3,4,5} F. Marino,^{4,6} G. Pandraud,⁷
G. A. Prodi,^{2,8} E. Serra,^{2,7,8} and M. Bonaldi^{1,2,*}

¹*Institute of Materials for Electronics and Magnetism, Nanoscience-Trento-FBK Division,
38123 Povo, Trento, Italy*

²*Istituto Nazionale di Fisica Nucleare (INFN), Trento Institute for Fundamental Physics and Application,
I-38123 Povo, Trento, Italy*

³*Dipartimento di Fisica e Astronomia, Università di Firenze, Via Sansone 1,
I-50019 Sesto Fiorentino (FI), Italy*

⁴*INFN, Sezione di Firenze, Via Sansone 1, I-50019 Sesto Fiorentino (FI), Italy*

⁵*European Laboratory for Non-Linear Spectroscopy (LENS), Via Carrara 1,
I-50019 Sesto Fiorentino (FI), Italy*

⁶*CNR-INO, Largo Enrico Fermi 6, I-50125 Firenze, Italy*

⁷*Department of Microelectronics and Computer Engineering/ECTM/DIMES,
Delft University of Technology, Feldmanweg 17, 2628 CT Delft, Netherlands*

⁸*Dipartimento di Fisica, Università di Trento, I-38123 Povo, Trento, Italy*

(Received 29 August 2014; revised manuscript received 10 February 2015; published 22 May 2015)

We present an oscillating micromirror with mechanical quality factors Q up to 1.2×10^6 at cryogenic temperature and optical losses lower than 20 ppm. The device is specifically designed to ease the detection of ponderomotive squeezing (or, more generally, to produce a cavity quantum optomechanical system) at frequencies of about 100 kHz. The design allows one to keep under control both the structural loss in the optical coating and the mechanical energy leakage through the support. The comparison between devices with different shapes shows that the residual mechanical loss at 4.2 K is equally contributed by the intrinsic loss of the silicon substrate and of the coating, while at higher temperatures the dominant loss mechanism is thermoelasticity in the substrate. As the modal response of the device is tailored for its use in optical cavities, these features make the device very promising for quantum-optics experiments.

DOI: 10.1103/PhysRevApplied.3.054009

I. INTRODUCTION

The research in cavity optomechanics [1] has been gathering a lot of momentum during the last couple of years, driven by the first observation of quantum phenomena. We mention, in particular, nonclassical behavior of optically cooled nanomechanical oscillators [2–8], radiation-pressure shot noise on a macroscopic object [9], and ponderomotive light squeezing [10–12]. Besides its indubitable interest for fundamental research (in particular, for exploring the classical-to-quantum border), this quantum breakthrough is opening the way to integrated systems implementing quantum measurements in sensing devices (e.g., for high-sensitivity detection of position, acceleration, force, mass, etc.) [13], as well as to the use of optomechanics in quantum interconnects [14–16] and quantum memories [17].

Beyond the first achievements, research work aiming to improve and extend the existing platforms is particularly important, in view of possible applications. In fact, low-frequency squeezing could be useful for improving the sensitivity of audio-frequency measuring devices such as

magnetic-resonance force microscopes [18]. We remark that, in recent pioneering works, the injection of squeezed light generated by an optical parametric oscillator has been successfully employed to operate gravitational-wave detectors beyond the quantum shot-noise limit in the frequency region down to 150 Hz [19,20]. However, meaningful ponderomotive squeezing has been obtained in the MHz range [11,12] and is much more difficult to achieve at lower frequencies, due to detrimental effects from various sources of technical noise [10], so that the research must be supported by the development of dedicated devices. In this article, we present a silicon-based micro-oscillator with high-reflectivity coatings, to be used as an end mirror in an optical cavity. Our purpose is to produce a device capable of generating radiation squeezing and quantum correlations in the ~ 100 -kHz region, and characterized by high reproducibility to allow inclusion in integrated systems.

From the beginning, the development of this system requires the meeting of conflicting requirements, and several prototypes were built to evaluate the effectiveness and the feasibility of specific solutions. Actually, our previous generation devices allowed us to demonstrate useful physical effects, such as frequency-noise cancellation [21], parametric modulation and stabilization of the

*bonaldi@science.unitn.it

optical spring [22], and optimal filtering and detection [23]. However, in spite of the continuous progress [24,25], the system's quality factor is still far from optimal, and they showed residual coupling with the wafer modes, energy leakage through the supporting structure (clamping losses), and performance strongly affected by the supporting system. On the contrary, the device presented here solves all technical issues specifically related to the device. Thanks to an integrated nodal suspension, a quality factor up to 1.2×10^6 is reliably obtained at cryogenic temperatures together with optical losses lower than 20 ppm. A set of measurements with different devices in the temperature range 4–300 K allows us to distinguish the main causes of the residual dissipation and confirms the assumptions and simulations at the base of the design. Therefore, the device represents our ultimate candidate for quantum measurements in this frequency band.

In Sec. II, we set the technical requirements and in Sec. III we describe the guidelines of the design process. We describe in some detail the dissipative phenomena at work in this type of oscillator, using the engineering point of view, where each dissipative phenomenon must be simply controlled, and we refer to the literature for the fundamental aspects. In some cases, as a comparison, we describe results obtained with nonoptimal oscillators, which are useful for understanding the necessity of the currently adopted solutions. Given that the actual observation of quantum optomechanical effects critically depends on a number of parameters of the whole experimental configuration, we deal also with aspects related to the integration of the device with the optical system used to generate and detect light, including the thermal design of the system and the dynamic effect of the integrated seismic isolation. In Sec. IV, we summarize the microfabrication of the devices, with a focus on the procedure needed to integrate the optical coating in the microelectromechanical systems (MEMS) fabrication process. In Sec. V, we describe the experimental characterization of the device.

II. MAIN REQUIREMENTS

A. Noise balance

We assume that the oscillating micromirror, with effective mass M , angular frequency Ω_m , and quality factor Q , works as an end mirror in an optical Fabry-Perot cavity operating at temperature T . Some fundamental requirements for the oscillator may be obtained by comparing the power spectral density (PSD) of the radiation-pressure noise with the PSD of the thermal noise. As a general criterion, we require that the radiation-pressure-force noise due to quantum fluctuations must dominate over the thermal equivalent force noise [26,27],

$$\hbar\omega_L P_{\text{in}} \frac{4}{c^2} \left(\frac{2T}{T + \mathcal{L}} \right)^2 \left(\frac{\mathcal{F}}{\pi} \right)^2 > 2k_B T \frac{M\Omega_m}{Q}, \quad (1)$$

where \mathcal{T} and \mathcal{L} are the input mirror intensity transmission and the cavity losses, respectively, the finesse is defined as $\mathcal{F} = 2\pi/(\mathcal{T} + \mathcal{L})$, ω_L is the angular frequency of the laser, and P_{in} its input power. This relation is valid in the experimental configuration of bad cavity (cavity linewidth much larger than the mechanical oscillation frequency) and for vanishing detuning.

Equation (1) gives an order-of-magnitude estimate of the regime where the generation of squeezed light can be obtained as a result of the quantum optomechanical correlations between field quadratures. Focusing on the right-hand side, we see that the thermal noise should be minimized by reducing the effective mass of the resonator, its frequency, and by enhancing the quality factor Q ; a base temperature as low as possible is highly recommended. From the left-hand side, we see that \mathcal{F} should be enhanced together with the laser input power P_{in} , provided that the device is capable of dissipating the resulting power with a tolerable temperature increase (see Sec. III E).

B. Optical losses

There are three main contributions to optical losses: first, coating defects (such as roughness and inhomogeneity) scatter the light, thus leading to the attenuation of the reflected power; second, the coating partially absorbs the impinging light; and third, the finite size of the mirror gives rise to absorption and diffraction of the beam fraction that hits the device out of the coated part. The scatter loss can be related to the rms roughness of the surface through the total integrated scatter, that is, the ratio of the integrated scatter power to the reflected specular power, evaluated from Davies's formula [28,29],

$$\mathcal{L} = \mathcal{A} + \mathcal{D} + \left(\frac{4\pi}{\lambda_0} \right)^2 \sigma^2, \quad (2)$$

where λ_0 is the wavelength (for our Nd:YAG laser $\lambda_0 = 1064$ nm), \mathcal{A} and \mathcal{D} are the contributions to the total optical losses of absorption and diffraction due to finite mirror size, respectively, and $\sigma^2 = \int W(\mathbf{r}) d(\mathbf{r}) d^2\mathbf{r}$. Here $d(\mathbf{r})$ stands for the differences between the mirror surface and the ellipsoidal best-interpolated surface; $W(\mathbf{r})$ is the Gaussian weight corresponding to the laser-beam intensity on the mirror, $W(\mathbf{r}) = (2/\pi w_0^2) \exp(-2r^2/w_0^2)$, with w_0 the waist of the Gaussian beam.

This equation sets the constraint on the roughness of the wafer according to the desired cavity specifications. We assume a laser waist of ~ 50 μm and require loss \mathcal{L} lower than ≤ 20 ppm. If the mirror has a diameter of at least 250 μm , corresponding to 5 to 6 times the laser waist, diffraction losses are negligible ($\mathcal{D} < 1$ ppm) and a rms roughness lower than 0.5 nm is necessary.

C. Squeezed-light generation

Given that essential technological requirements for this device are low optical and mechanical losses, more

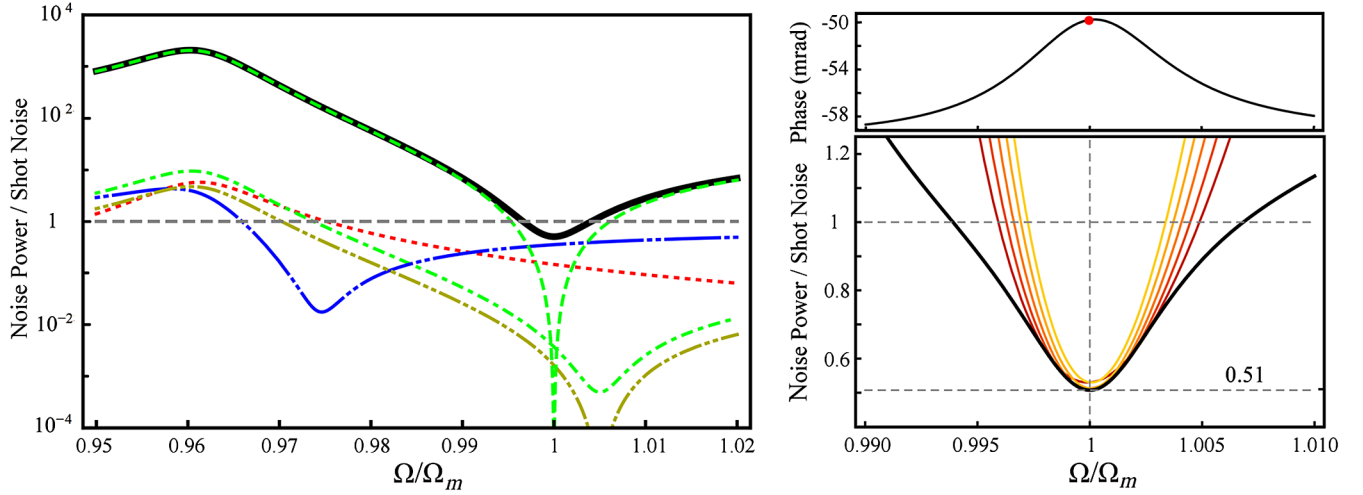


FIG. 1. Left panel: calculated noise spectrum of the radiation reflected by the optomechanical cavity, normalized to its shot-noise level, for a laser detuning $\delta = -0.03$. The detection phase is 50 mrad and the physical parameters are those measured in the present work. The solid line shows the total noise; the other lines distinguish the different contributions: frequency noise and background displacement noise (green dashed line), thermal noise (red dotted line), vacuum noise (blue dash-double-dotted line), laser-amplitude quantum noise (green dash-dotted line), and excess laser-amplitude noise (olive dash-double dotted line). The radiation noise falls below its standard quantum level around the bare mechanical resonance (at $\Omega = \Omega_m$). Right panel: enlarged view. The different curves from yellow to red correspond to steps of 1 mrad in the detection phase, keeping constant all other parameters, and show that some uncertainty or fluctuations in the detection phase are acceptable. The black solid curve shows the maximum quantum noise reduction achievable as the detection phase is optimized at each frequency. The detection phase necessary to obtain such optimum squeezing curves is shown in the phase graph, where a red dot marks the value used for the curves in the left panel, while allowing the lowest achievable noise level of 0.51.

complete calculations are necessary to determine if ponderomotive squeezing (and similar quantum effects) can be produced and revealed [30]. We perform these calculations using a quantum Langevin model (described, e.g., in Ref. [21]), with the parameters measured in the present work: $\Omega_m/(2\pi) = 140$ kHz, $M = 2.3 \times 10^{-7}$ kg, $Q = 1.2 \times 10^6$, $T = 100$ ppm, $\mathcal{L} = 40$ ppm, cavity length 1 mm, $P_{\text{in}} = 10$ mW, $T = 4.5$ K, relative intensity noise (RIN) = -167 dB, laser frequency noise $1 \text{ Hz}^2/\text{Hz}$, and background displacement noise $8 \times 10^{-35} \text{ m}^2/\text{Hz}$. A meaningful squeezing seems indeed attainable with an input laser power of 10 mW (and an intracavity power of 200 W), as shown in Fig. 1. Here, the radiation noise falls below its standard quantum level in a frequency range around the bare mechanical resonance (at $\Omega = \Omega_m$), thanks to the cancellation of the background noise [21], even for relatively large (and therefore less critical) values of laser detuning ($\delta = -0.03$) and detection phase (50 mrad). We note that, with these parameters, the general criterion given in Eq. (1) shows that the radiation-pressure-force noise is about 1.6 times the thermal equivalent force noise.

A crucial issue for a realistic assessment of the experimental conditions is the system stability, that must be evaluated taking into account the combined photothermal and ponderomotive effects [31,32]. For the parameters under consideration, the system is stable in the whole region of negative δ , where δ is the laser detuning normalized to the cavity half-linewidth. For intracavity power of ~ 300 W, a null-width instability region appears at

$\delta = -0.575$. It becomes wider at increasing power, but at 800 W the system is still stable for $-0.1 < \delta < 0$.

As for the laser noise, we consider a frequency noise of $1 \text{ Hz}^2/\text{Hz}$ (a conservative value according to our measurements) and a relative intensity noise of -167 dB. The latter is the RIN level that we obtain with an external noise eater, based on an electro-optic modulator and a polarizer [33], from the initial RIN of -140 dB. At 10 mW, the Mandel parameter [34] is 0.5.

III. DESIGN RATIONALE

As we have seen in the previous section, a high finesse (and therefore high mirror reflectivity) is needed to maximize the force per incoming photon exerted by the cavity field on the mechanical element. A high mechanical quality factor is useful to improve the element's response to the radiation-pressure force and, at the same time, to decrease the influence of the thermal bath.

These requirements are quite common in the design of precision instruments, and general strategies have been developed in the past to control optical [35] and mechanical losses [36]. As for optical microsystems, several groups have indeed explored designs of micromirrors oscillating in the range of frequencies we are considering [37–40]. In all cases, it is evident that it is very difficult to satisfy, at the same time, all the technological requirements necessary for the observation of quantum effects. On the basis of what we observed in our previous series of oscillators, the main problems came from the mechanical side of the system.

A. Material selection

It is well known that large single-crystal silicon mechanical resonators ($10 \times 10 \times 10 \text{ cm}^3$) can show loss angles as small as $Q^{-1} = 10^{-9}$ at liquid-helium temperatures. For smaller systems, this figure reduces with the characteristic size [41], due to the intrinsic dissipation mechanisms characterizing microscopic structures at low temperature. Therefore, for a device with a characteristic size of about $100 \mu\text{m}$, it is possible to obtain the needed loss angle of $Q^{-1} = 10^{-6}$ [42].

Further advantages of silicon are the negligible thermoelastic dissipation at low temperature, and a high thermal conductivity, which allows one to easily cope with the problem of power handling. This is combined with the wide availability of high-quality crystal wafers and of well-proven process technologies.

With regard to the optical coating, we decided to use a Bragg reflector of alternate $\text{Ta}_2\text{O}_5/\text{SiO}_2$ quarter-wave coating layers (see also Sec. IV). This coating can reach optical losses as low as a few ppm, but it is quite lossy from the mechanical point of view. The main challenges of the proposed device are the integration of the optical coating within a MEMS production process and the development of a design which allows us to preserve high mechanical quality factors.

B. Coating mechanical-loss control

The structural dissipation is directly related to the imaginary part of Young's modulus in a material, and a loss angle of about $\phi_c = 5 \times 10^{-4}$, independent from the temperature, is expected for the high-reflectivity coating layer [43]. Consequently, the quality factor of a resonator engraved entirely from the coating layer would be not greater than a few thousand. In fact, for each resonant mode, the loss angle can be written as $\phi_t = \Delta W_t / 2\pi W_t$, where W_t is the energy stored in the resonant mode and ΔW_t is the total energy loss per oscillation cycle. The quality factor of the mode is simply $Q_t = \phi_t^{-1}$. When the resonator is made by different materials, the energy dissipation is determined by a combination of various mechanisms which dominate in each subsystem of the oscillator. Because rigidly moving parts do not dissipate strain energy, the total loss is given by the sum of the loss angle of each subsystem, weighted by the corresponding strain-energy ratio. In our case, with a silicon spring and a coated mirror,

$$Q_t^{-1} = \phi_s \frac{W_s}{W_t} + \phi_c \frac{W_c}{W_t}, \quad (3)$$

where W_s and W_c are the strain energy stored in the silicon and in the coating, respectively. According to this relation, the loss due to the coating can be reduced if the associated strain energy is made negligible with respect to the total energy of the resonator. For this reason, in our resonators, the mirror is positioned on a part moving as rigidly as

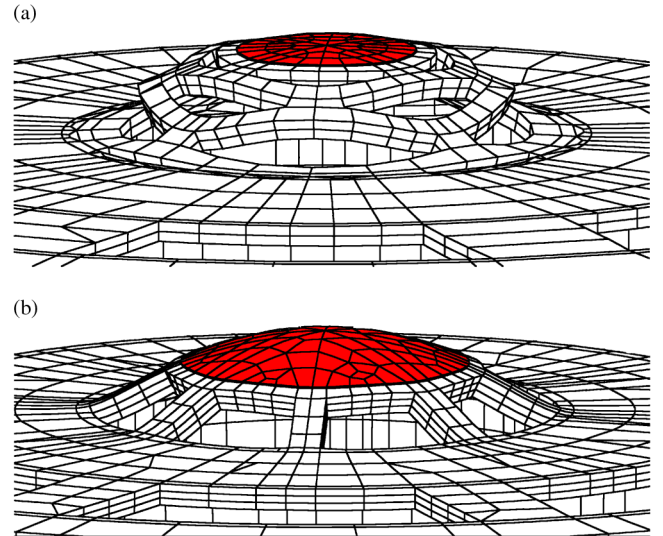


FIG. 2. Modal shape of the fundamental mechanical mode of two devices. The central red circle indicates the area covered with the reflective coating. The amplitude of the displacement is exaggerated for clarity. (a) Low-deformation mirror design: the structure made of alternating torsional and flexural springs allows an almost rigid vertical displacement of the coated area. (b) Standard design [24]: radial flexural springs induce a significant bending in the disk.

possible, to reduce the strain energy stored in the coating layer [24]. As shown in Fig. 2(a), the central mirror is supported by a structure made of alternating torsional and flexural springs. This allows a vertical oscillatory motion with minimal deformation during the displacement. In contrast, when the mirror is supported by standard radial flexural springs [Fig. 2(b)], the bending of the flexural members induces comparable bending in the central disk. In this case, the deformation during the motion is about 1 order of magnitude higher.

The energy ratios for each modal shape can be easily evaluated by a finite-element (FE) study; therefore, the resulting total loss can be predicted from the loss angle of the coating and of the silicon substrate. Typical agreement of this procedure with experimental data is 20% [24]. Given the diameter of the mirror needed to obtain the required cavity finesse, the mechanical micro-oscillators are conceived to confine the high-reflectivity coating on a part moving as rigidly as possible. We tested the effectiveness of this design procedure in a previous version of the optomechanical devices [25].

C. Isolation wheel and nodal suspension

The performance of resonant devices is often affected by poor experimental reproducibility of the mechanical losses. These can depend not only on the intrinsic characteristics of the oscillator or its environment, but also on the specific clamping method used to attach the resonator to the support. In fact, with some resonator designs, the maximum

strain of the vibrational mode can arise at the clamping zone. As a result, a large fraction of the total elastic energy is located there and is dissipated in the sample holder. This originates an additional contribution to the loss of the vibrational mode which commonly overwhelms the internal losses.

To allow a predictive approach to the problem, we incorporate a filtering structure in the microfabricated device. This choice allows a comprehensive finite-element study of the system and this enables setting the minimal features of the on-chip isolation stages needed to make irrelevant (from the mechanical point of view) the characteristics of the external sample holder used to construct the cavity. This analysis reveals the effect of the vibrational shell modes of the silicon chip supporting the device. These modes, densely distributed in frequency, can very easily form hybrid modes with the optomechanical resonator and facilitate vibrational energy transfer toward the sample holder [25]. A second major issue is the recoil force required to balance the movement of the mirror, which is ultimately supported by the outer support, and then provides another channel for energy loss.

In Figs. 3(a) and 3(b), we show the drawing and some SEM details of a typical sample. The resonator is formed by the central mirror, covered by the optical coating, suspended by the elastic structure. The fabrication process is described in Sec. IV. As shown in Fig. 3(c), we can define

three main subsystems in the mechanical structure of the device:

- (1) the main oscillator engraved from the device layer of the SOI wafer. It is formed by the central mirror, the elastic structure that allows movement while maintaining low deformation of the coating layer, and four counterweights;
- (2) a massive inner frame obtained from the full thickness of the SOI wafer. This part acts both as nodal support for the main oscillator and as a seismic isolation stage; and
- (3) an outer suspended frame, mainly acting as an isolation stage from wafer and holder modes.

The double-frame geometry works as a cascaded resonant low-pass mechanical filter system with poles at about 30 and 60 kHz. In addition, the structure entails a vibrational mode that greatly reduces the energy leakage from the main oscillator toward the outer frame and then the supporting wafer. In fact, for the main oscillator mode shown in Fig. 3(d), the motion of the mirror is balanced by the motion of the counterweights. As a result, the total recoil on the inner frame is virtually zero and the outer frame does not take part in the motion at all. We are actually dealing with a nodal suspension, a design technique capable of reaching the highest level of isolation presented in the literature [44–46]. We remark that, despite the complexity of the structure, the main oscillator mode

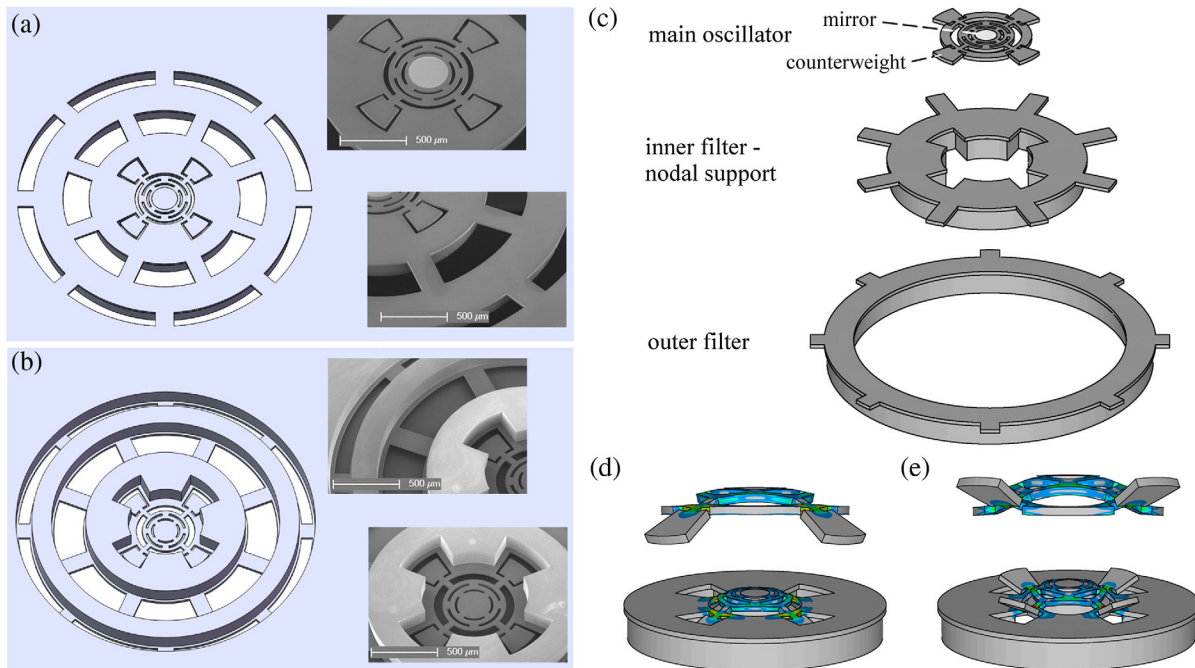


FIG. 3. Computer-aided design drawings and SEM details of two optomechanical oscillators, with resonant frequency of the main mode at 117 kHz and 150 kHz. (a) Front side, with the elastic structure etched in the device layer, and the circular mirror deposited over the central disk. (b) Back side of the second oscillator with the circular frame etched in the handle layer. (c) Main functional parts of the device. (d) Modal shape of the main oscillator mode: the motion of the mirror is balanced by the counterweights. (e) Modal shape of the antibalanced mode: the mirror and the counterweights move in phase. The contour plots show relative values of stress intensity in the structure, from zero (gray) to the maximum value (red) for each modal shape.

represents the first mode of the device, after the low-frequency modes of the isolation stages that exhibit a much higher effective mass.

The proper operation of the system is guaranteed by an accurate balancing of the counterweights, calculated by the use of specially developed FE tools. In Fig. 4, we show the ratio between displacements of the outer frame and of the mirror, evaluated for the main resonator mode as a function of the length of the counterweights. The case of zero-length counterweights is equivalent to the unbalanced old version of the device, where clamping loss limits the quality factor to $Q \approx 10^5$. The counterweight length from $366 \mu\text{m}$ to $379 \mu\text{m}$ (well within the resolution of the microfabrication) reduces by 1 order of magnitude the displacement ratio seen in the unbalanced case, with a correspondent 100-fold reduction of the energy stored in the outer frame during the motion and a similar reduction of clamping loss. The resulting total mass of the counterweights is about 10^{-7} kg, similar to the mass of the mirror. We point out that the weight of the optical coating, about 3×10^{-9} kg, also must be considered in the balancing procedure. As shown in Fig. 4, an oscillator with a bare

mirror would be optimally balanced with a counterweight about $8 \mu\text{m}$ shorter.

D. Effects of low-frequency modes

In an ideal optical apparatus, the cavity length varies only for the oscillations of the microresonator in its fundamental mode. Actually, the length of the cavity is also modulated by the internal modes of the support structure and of the input mirror, as well as by the spurious modes of the device. For this reason, strictly resonator-specific requirements (optical losses, mechanical losses, or conductivity of the materials used) are not sufficient to predict the behavior of an oscillator when inserted in the experimental apparatus. The overall behavior of the system is determined from the whole modal spectrum of the device, since each of the normal modes in the system contributes to the optomechanical transfer function of the system and is driven by thermal forces and environmental vibrations.

When a mechanical mode is outside the bandwidth of the lock circuit used at to stabilize the laser to the cavity resonance [the Pound-Drever-Hall (PDH) loop], its rms vibration must not exceed the cavity's dynamic range. Therefore, as a minimal stability requirement, we ask that the rms mechanical noise is well below the resonator linewidth; in our case, $\lambda_0/(4\mathcal{F}) \approx 2 \times 10^{-12}$ m. This condition can be easily matched in the case of thermal noise. In fact, the variance of the displacement contributed by each mode coupled to the cavity length is determined by the equipartition principle as $\langle x^2 \rangle_{\text{LF}} = k_B T / (M_0 \Omega_0^2)$, where M_0 is the effective mass [47] and Ω_0 is the resonant frequency. Given the mass and the frequency of the outer filter mode, we expect a total noise contribution of about 3×10^{-14} m at room temperature. On the other hand, with regard to the environmental vibrational noise, a white acceleration-noise spectra of amplitude $2a_0^2$ induces a vibrational noise with variance proportional to the quality factor of the mode,

$$\langle x^2 \rangle_a = a_0^2 \frac{Q}{2\Omega_0^3}, \quad (4)$$

that sets to about $10^{-6} \text{ m s}^{-2}/\sqrt{\text{Hz}}$ the admissible acceleration-noise spectral density at the frequency of the outer filter. This requirement on the vibrational-noise level can be met through the use of evacuated enclosures on top of isolated optical tables. On the other hand, if the experiment is performed in a cryogenic environment, the additional vibrations induced by the cooling system can easily exceed this limit.

A second point must be taken into account when inserting filter modes at low frequency. In fact, in the standard model for the cavity dynamics, the sign of the damping rate is determined by the detuning of the input field and, in particular, it is the same for every normal mode of the specific structure, despite their different coupling

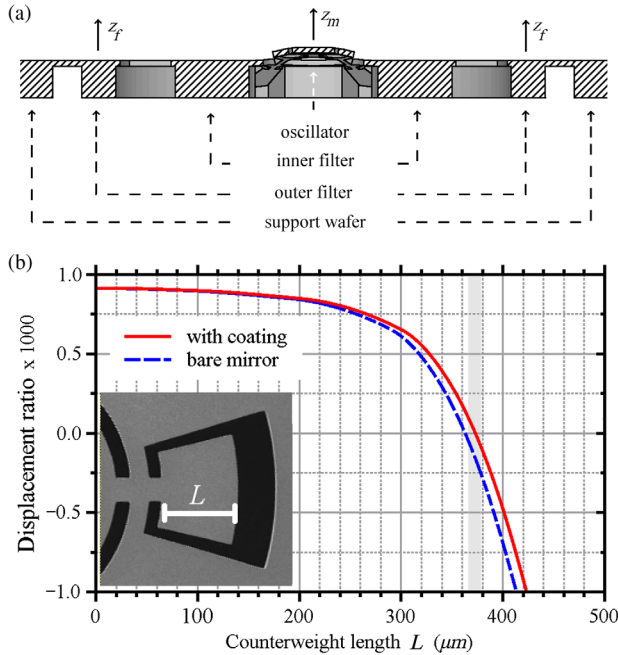


FIG. 4. The balancing procedure calculated by the FE method, giving the ratio of the amplitudes $D_r = z_f/z_m$ (area average) for the modal shape of interest. A small value of D_r indicates that the modal shape remains confined within the inner frame, reducing energy leakage toward the environment. (a) Section of the device. (b) Plot of the curves used to set the counterweights length L needed to balance the main oscillator mode. Red (solid) line represents the balance curve for the complete device; the light-gray band highlights the value of L for which $D_r < 10^{-4}$. Blue (dashed) line shows the balance curve for the device without optical coating.

strengths. When the cavity-locking system is included in the model, this is no longer true, and the most notable consequence is dramatically changing the landscape of the instability region. In this respect, we mention another class of silicon microresonators, where requirements on losses are satisfied thanks to the use high-order torsional modes [48,49]. However, the presence of lower-order modes makes these systems unsuitable for the use in high-finesse optical cavities, due to the onset of complex dynamical instabilities [50]. A thorough discussion of the dynamics of a multimodal optomechanical system goes beyond the scope of this paper, and we only note that the introduction of on-chip seismic isolation forces us to consider the effect of some fixed and reproducible isolation mode, with the advantage of isolating the system from poorly reproducible modes of the wafer and of the sample holder. Here, we summarize some general design guidelines that result in a stable system up to the needed optical power (as demonstrated by the results shown in Sec. V):

- (1) the main frequency mode of the resonator should be well separated (tens of kHz) from other internal modes of the silicon structure;
- (2) the isolation modes should have equivalent mass orders of magnitude larger than the equivalent mass of the mirror; and
- (3) the frequencies of the isolation modes should be placed at the same time well below the mirror's mode and well over the bandwidth of the PDH loop.

E. Power handling

We show that, to allow the detection of quantum optomechanical effects in the cavity dynamics, one must work at cryogenic temperature and, at the same time, must enhance the optomechanical coupling by the use of an intracavity power of about 200 W. To ensure the thermal stability of the system, we assess by FE simulation the efficiency of the device for dissipation of the heat produced by the fraction of light power absorbed by the mirror. The absorbed power in a resonant Fabry-Perot cavity is $(4T/(T + \mathcal{L})^2)AP_{\text{in}}$. Typically, in our experiments, we measure $\mathcal{A} \approx 4$ ppm [51], $\mathcal{L} \leq 40$ ppm, and we consider $T \approx 100$ ppm. With these figures, in our cavity, an absorption of 1 mW implies an input power as large as 12 mW, with 250 W of intracavity power. These parameters are also used to evaluate the noise budget shown in Fig. 1 and satisfy the general criterion given in Eq. (1).

We calculate the temperature distribution in a typical device when the background is kept at liquid-helium temperature and when 1 mW of laser power is absorbed by the mirror. The steady-state thermal simulation (Fig. 5) shows that the oscillator remains at 4.3 K, thanks to its relatively large thickness and to the high thermal conductivity of silicon [52]. Moreover, the temperature is fairly homogeneous within the oscillators, with a maximal temperature spread of about 0.1 K.

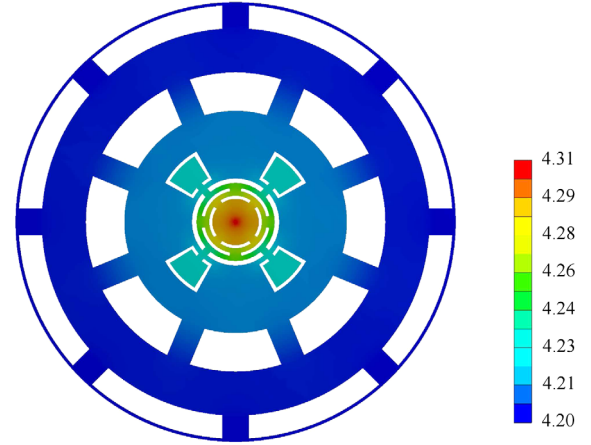


FIG. 5. Simulated temperature distribution on the microresonator shown in Fig. 3(a). The temperature background is fixed at 4.2 K (liquid-helium temperature) and an absorbed power of 1 mW is applied on a circular surface of diameter 0.1 mm at the center of the mirror.

From this result, it is clear that, from the thermal point of view, even a larger dissipated power could be properly managed at liquid-helium temperature. We remark that typical thermal-conductivity values for high-purity-silicon crystals at 4.2 K is well above 100 W/(K m), but this figure drops by many orders of magnitude at ultracryogenic temperatures. Moreover, geometrical effects could further reduce the thermal conductivity of the structure at low temperatures. The useful working range of our devices is therefore limited to temperatures well above 1 K, if a substantial optical power is required.

IV. MICROFABRICATION

The process developed for the fabrication allows one to integrate a high-reflectivity optical coating in a micromachined silicon oscillator. We briefly summarize the fabrication procedure, referring to specific technical publications for the details of the process.

We built 12 different versions of the design, resonating in the range 100–200 kHz and with equivalent masses of $1\text{--}4 \times 10^{-7}$ kg. The diameter of the mirrors ranges from 400 to 620 μm and allows negligible diffraction losses even in noncritical cavities (i.e., without being obliged to an ultrashort or a near-hemispherical configuration). For the microfabrication, we used silicon on insulator (SOI) wafers made of a $70 \pm 1 \mu\text{m}$ $\langle 100 \rangle$ -device layer and $400 \pm 5 \mu\text{m}$ -thick handle wafer [Fig. 6(a)]. Wafers are high-purity floating-zone phosphorus-doped with a resistivity value greater than 1 k Ω cm. The rms surface roughness of the device layer is about 0.5 nm, measured over an area of $100 \times 100 \mu\text{m}^2$. The fabrication exploits MEMS bulk micromachining by deep-reaction ion etching (DRIE) and through wafer two-side processing [53]. The suspended resonating part is derived from the device layer

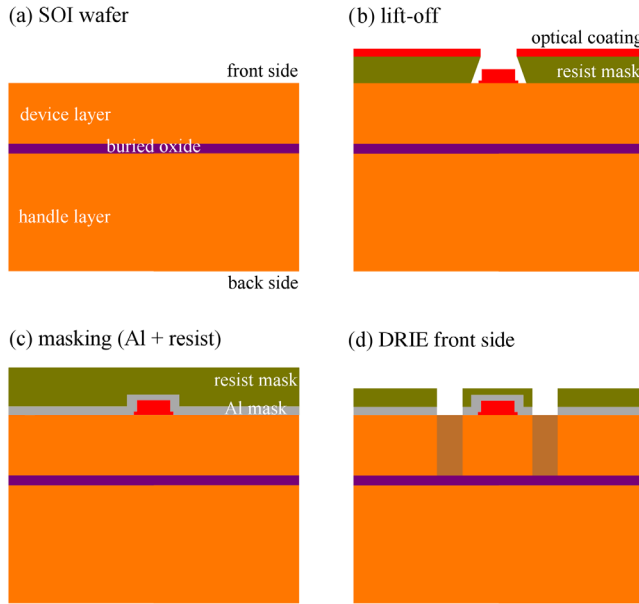


FIG. 6. (a) Initial SOI wafer. (b) Optical coating deposition and lift-off. (c) Protection and masking of the mirror. (d) DRIE step to obtain front-side structure.

of the SOI wafer, while filters are fabricated from the full wafer thickness. The buried oxide layer that separates the device layer from the handle wafer is $1 \pm 0.5 \mu\text{m}$ thick and used as an etch stop layer for the two-side DRIE process.

The optical coating is deposited on the wafer before the silicon micromachining [Fig. 6(b)]. The high-reflective-coating deposition is done at the ATFilms-IDEX facility. The mirror is a Bragg reflector of 38 alternate $\text{Ta}_2\text{O}_5/\text{SiO}_2$ quarter-wave coating layers for a total thickness of $5.9 \mu\text{m}$, deposited by ion beam sputtering. The shape of the mirrors is defined by a lift-off procedure: the resist is removed by a hot acetone solution and the coating is stabilized by annealing at 430°C . The nominal coating reflectivity at 1064 nm is 99.9995% . No variations from the native roughness are observed in the wafer after this process step. The optical coating is then covered by a layer of pure Al deposited at low temperature, an additional resist layer is applied by spin coating [Fig. 6(c)]. This protection layer is patterned to define the front side of the structure in the following DRIE step [Fig. 6(d)], where the buried oxide is used as stop-etch layer. The mechanical structures in the handle layer are then obtained by a single DRIE step on the back of the wafer. A standard alignment procedure is applied to guarantee proper matching of the two side process.

We point out that DRIE is a critical step in the micro-fabrication of high-aspect-ratio structures. The etching recipe must be carefully calibrated to avoid (1) local etch-rate variations (e.g., when a large feature has a greater depth than an adjacent small feature), (2) systematic variation of etch rate across the wafer, and (3) formation

of residue silicon spikes. At the end of the DRIE process, the wafers are first cleaned from resist residues by oxygen plasma and a HNO_3 solution, then the buried oxide layers are removed by a BHF solution. As a last step, the protection Al layer is etched and the wafers are cleaned in water.

V. EXPERIMENTAL RESULTS

A. Vibration spectrum

In Fig. 7, we show the vibration spectrum of the oscillator at room temperature, acquired with a 1-mm-long Fabry-Perot cavity with the micromirror as an end reflector, using the phase-modulation technique with a weak probe beam [53]. The cavity is ideally sensitive only to displacements of the mirror along its axis (z_m in Fig. 4), although a sensitivity to rotations around the x or y axis (rocking modes) is induced when the laser beam is not perfectly centered on the mirror. The experimental curve shows the low-frequency filter mode at 24 kHz and a noisy region around 75 kHz , corresponding to coupled vibrations of the filtering frames. The oscillator modes, balanced [Fig. 3(d)] and antibalanced [Fig. 3(e)], are at 141 and 181 kHz , respectively. The noise floor of the cavity readout is measured with a fixed mirror mounted in place of the device, and it is shown as a gray band in Fig. 7; it ranges from 10^{-33} to $10^{-34} \text{ m}^2/\text{Hz}$, depending on frequency. We show also the expected thermal-noise spectrum evaluated by a FE study. In the simulation, we assign to the oscillator a loss angle 2×10^{-5} ($Q \approx 5 \times 10^4$), determined by thermoelastic loss in silicon at room temperature [36]. The energy loss through the clamping system is modeled by assigning a loss angle 10^{-3} to the filter modes,

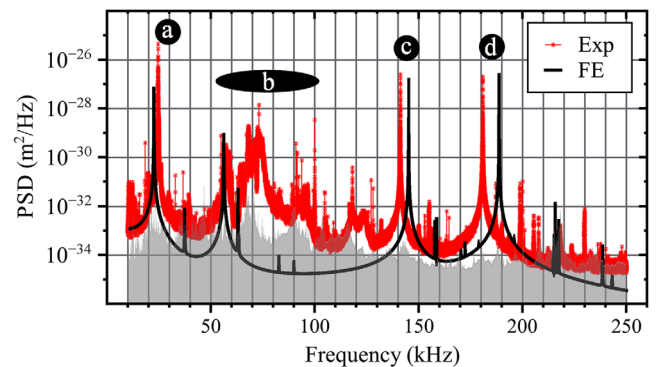


FIG. 7. Noise power spectral density (PSD) of the cavity output at room temperature. Red curve: experimental data. Black line: expected displacement thermal-noise spectrum evaluated by FE simulation. Light-gray shaded region: noise floor of the cavity readout. The letters identify the main features of the noise spectrum of the device. (a) Low-frequency filter mode; (b) coupled vibrations of the filtering frames (a centered laser beam and ideal constraints are used in the simulation, therefore, the sensitivity to rocking modes is greatly reduced in the FE curve); (c) main oscillator mode; and (d) antibalanced oscillator mode.

corresponding to a much lower quality factor $Q \approx 10^3$. With this choice, the agreement with the experimental data is, however, only qualitative for the filter modes. In fact, the model does not account for the details of energy transfer between the filters and the clamping system, nor for the thermal vibration of the sample holder and the input mirror. Moreover, the filters are obviously driven by the acoustic and vibrational noise in the laboratory. We observe instead that the vibration spectrum of the oscillator mode, thanks to the low-pass filters and to the nodal suspension, is in good agreement with the FE predictions for a system subject only to thermal forcing. These findings underline that an effective mechanical isolation is useful both to reduce vibrational noise and to improve the quality factor of an oscillator.

Figure 7 also highlights a further important feature of the device, namely that in the low-frequency range (up to the main oscillator mode) only the filters' vibration modes are present. Given that these modes are about 100 times heavier than the main oscillator mode, they do not affect significantly the cavity stability region [50] and allow one to reach the sensitivity floor at the oscillator frequency. The possibility to operate in a high-finesse cavity with relevant input power is demonstrated by the spectra in Fig. 8. Here $\mathcal{T} \approx 300$ ppm and the cavity is strongly overcoupled ($\mathcal{F} \approx 18\,000$, $\mathcal{L} \approx 40$ ppm). An additional strong beam, weakly detuned, modifies the resonance frequency and width of the oscillator main mode by optomechanical coupling. The input power of 20 mW gives an intracavity power of 210 W, and the system maintains excellent stability. The offset of the fitting Lorentzian curves gives a noise floor of 8×10^{-35} m²/Hz. We note that this configuration is not optimized for the observation of ponderomotive squeezing, which is instead favored by an input mirror with $\mathcal{T} \approx 100$ ppm and 10 mW input power, as described in Sec. II C and Sec. III E.

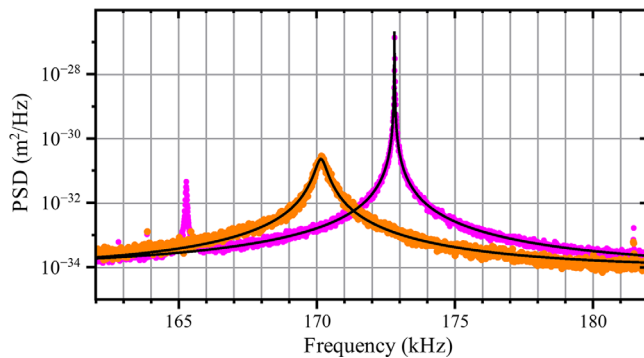


FIG. 8. Noise PSD of the main oscillator mode at room temperature, in the regime of high intracavity power. With respect to Fig. 7, here the device has higher oscillation frequencies. Violet dots indicate a weak probe beam. Orange dots denote an additional beam, of input power $P_{\text{in}} = 20$ mW. Black lines show Lorentzian fitting functions.

B. Mechanical-loss measurement

The mechanical characterization is performed in a cryostat, operating in the full range 4.2–300 K. To avoid optical cooling effects from the cavity setup, we use a Michelson interferometer to characterize the oscillators, measuring the decay time after a strong resonant excitation of the support with a piezoelectric crystal. In Fig. 9, we show the loss angle of the main oscillator mode as a function of the temperature. Recall that the total loss angle (equivalent to $1/Q$) is simply the sum of all losses effective in the elastic structure, and its evaluation allows one to distinguish in the experimental data the typical features of dissipative effects acting in the system.

It is apparent that the performance of the oscillator is much improved from the previous version of the device. Indeed, the results of the loss measurements are very scattered in samples without counterweights, depending on the details of the clamping used in the experiment. The best result obtained at 4.2 K with a complete device (two low-pass filters with counterweights) is a loss angle $\phi \approx 8.3 \times 10^{-7}$ ($Q \approx 1.2 \times 10^6$). This value is more than 1 order of magnitude better than in our previous design [25], and is fully within the requirements for the detection of quantum effects with our apparatus. We also remark that test samples with nodal suspension, but lacking the external filtering wheel (not represented in the figure), exhibit loss angles higher by roughly a factor of 2. Therefore, only the complete device allows one to achieve the best performance. Moreover, it is worth noting that the reduction of the loss from the clamping and from the coating layer allows the observation of the thermoelastic loss in the silicon structure, as demonstrated by the presence of the typical dip at 124 K (where the coefficient of thermal expansion of silicon drops to zero).

The performance of a test device optimized without optical coating allows us to estimate the ultimate potential

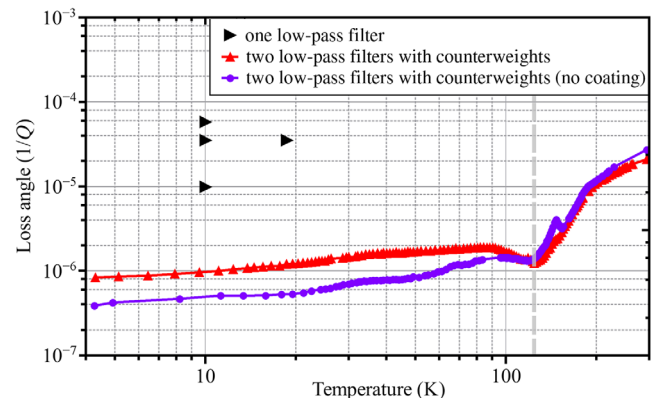


FIG. 9. Loss angle of a complete device (two low-pass filters with counterweights) and a test device without coating. Samples without nodal suspension (one low-pass filter) correspond to an old version of the device [25]. Thermoelastic loss nulls at 124 K (dashed vertical line) and originates a dip in the loss angle.

TABLE I. Experimental parameters of a typical optomechanical device. Ω_m is the angular frequency of the main mode and M its effective mass, estimated from thermal-noise measurements at room temperature [24]. The quality factor Q is measured from the decay of free oscillation. The finesse \mathcal{F} is measured in a ~ 1 -mm-long Fabry-Perot cavity with the micromirror as an end reflector and an input-coupler transmission of $\mathcal{T} = 50$ ppm [53]. The cavity losses calculated from \mathcal{F} and \mathcal{T} are $\mathcal{L} \approx 20$ ppm. According to the criterion given in Eq. (1), with this input coupler, the radiation-pressure-force noise is about 6.6 times the thermal equivalent force noise. We report also a number of optomechanical figures of merit, derived from these measured data, useful for direct comparison with other architectures and experimental implementations [1]. $\Gamma_m = \Omega_m/Q$ and κ are the mechanical and optical dissipation rates, respectively; the product $Qf = Q\Omega_m/(2\pi)$ measures the degree of decoupling from the thermal environment; κ/Ω_m is the sideband suppression factor, and g_0 is the bare optomechanical coupling rate.

T (K)	\mathcal{F} $\pm 10\%$	$\Omega_m/2\pi$ (kHz) $\pm 1\%$	M (kg) $\pm 10\%$	Q $\pm 10\%$	$\Gamma_m/2\pi$ (Hz)	Qf	$\kappa/2\pi$ (Hz)	κ/Ω_m	$g_0/2\pi$ (Hz)
295 ± 5	9.0×10^4	141	2.3×10^{-7}	4.7×10^4	3.0	6.6×10^9	1.7×10^6	11.9	6.4
4.3 ± 0.1				1.2×10^6	0.12	1.7×10^{11}			

and the effectiveness of this technological platform. It achieves the best performance with a loss of 3.6×10^{-7} ($Q = 2.8 \times 10^6$) at 4.2 K. Also, in this case, the thermo-elastic-loss dip is clearly visible in the temperature-dependent data. From the comparison with the complete device, we can roughly [54] estimate as 5×10^{-7} the loss contributed by the structural dissipation in the optical coating. This value is much lower than the typical loss angle in the coating, that is around 6×10^{-4} [24,43], and confirms the efficiency of the low-deformation mirror design.

Useful information can also be gathered from the study of the antibalanced mode [Fig. 3(e)], resonating at a frequency about 15% higher than the main mode. Actually, in the antibalanced mode, the mirror and the counterweights move in phase, eliminating the effectiveness of the nodal support. In this case, we measure a loss angle about 1 order of magnitude higher than in the corresponding balanced mode, with large variations typical of the phenomenon of clamping loss.

We summarize in Table I the experimental parameters of the optomechanical device. The results are consistent with the overall trend of the size dependence of loss in bare silicon micro- or nanomechanical oscillators [42], and confirm the effectiveness of the strategies employed to get rid of clamping loss and to integrate a lossy functional component (optical coating) in a low-loss mechanical oscillator.

VI. DISCUSSION AND CONCLUSIONS

According to the estimate shown in Sec. II C, the integration of the devices described in this paper in a properly designed optical system operating at cryogenic temperatures can allow similar squeezing levels to that achieved in a system based on a silicon nitride (SiN) resonant membrane [12]. In addition, the data reported in Table I make it possible to evaluate the performance of the device for different optomechanical tasks and to compare with other experimental approaches reviewed in Ref. [1]. For instance, given

that full coherence over one mechanical period is obtained when $Qf > k_B T / (2\pi\hbar)$, we note that our devices fulfill the minimum requirement for quantum optomechanics at cryogenic temperature, where $Qf > 8 \times 10^{10}$. On the other hand, expected performance in experiments on single photons and phonons are limited, given the relatively high mass of the oscillating mirror. This is also evident from the low value of g_0/κ .

With respect to the resonators based on stressed silicon membranes [55], we note that membranes reach quality factors up to 10^7 even at room temperature and have the advantage of being very light. However, in view of possible applications at frequencies below 100 kHz, it is not easy to reduce their frequency without losing the beneficial effects of internal stress on the quality factor. It must be also noted that these membranes are strongly coupled with their supporting frame, and lower-order modes display a considerable sensitivity of the quality factor from chip-mounting conditions [56].

In conclusion, we design, realize, and characterize micro-optomechanical systems conceived to work in the ~ 100 kHz range. The structure includes several particular features, such as structured beams, filtering stages, and in particular nodal suspensions obtained by balanced counterweights. The resulting mechanical performance achieves the intrinsic limit of silicon dissipation, thus getting rid of mechanical losses induced by the clamping and by the high-reflectivity dielectric coating. The mechanical susceptibility of the device is tailored for its use in optical cavities with high intracavity power, and its thermal design allows the simultaneous cooling of the system down to liquid-helium temperatures.

Thanks to the fabrication procedure (fully including the coating deposition), the devices are particularly suitable for the implementation of integrated systems exploiting quantum technologies. Further applications include tailoring of squeezed light in the acoustic band [57]. Possible improvements of the devices rely on the use of low-loss materials in the microfabrication, such as diamond for the substrate [58] or crystalline coatings [59].

ACKNOWLEDGMENTS

This work has been supported by MIUR (PRIN 2010-2011, Project No. 20109FPLWN) and by INFN (HUMOR project). A. B. acknowledges financial support by MIUR (FIRB-Futuro in Ricerca 2013, Project No. RBFR13QUVI).

-
- [1] M. Aspelmeyer, T. J. Kippenberg, and F. Marquardt, Cavity optomechanics, *Rev. Mod. Phys.* **86**, 1391 (2014).
- [2] A. D. O’Connell *et al.*, Quantum ground state and single-phonon control of a mechanical resonator, *Nature (London)* **464**, 697 (2010).
- [3] J. D. Teufel, T. Donner, D. Li, J. W. Harlow, M. S. Allman, K. Cicak, A. J. Sirois, J. D. Whittaker, K. W. Lehnert, and R. W. Simmonds, Sideband cooling of micromechanical motion to the quantum ground state, *Nature (London)* **475**, 359 (2011).
- [4] J. Chan, T. P. Mayer Alegre, A. H. Safavi-Naeini, J. T. Hill, A. Krause, S. Gröblacher, M. Aspelmeyer, and O. Painter, Laser cooling of a nanomechanical oscillator into its quantum ground state, *Nature (London)* **478**, 89 (2011).
- [5] E. Verhagen, S. Deléglise, S. Weis, A. Schliesser, and T. J. Kippenberg, Quantum-coherent coupling of a mechanical oscillator to an optical cavity mode, *Nature (London)* **482**, 63 (2012).
- [6] T. P. Purdy, R. W. Peterson, P.-L. Yu, and C. A. Regal, Cavity optomechanics with Si_3N_4 membranes at cryogenic temperatures, *New J. Phys.* **14**, 115021 (2012).
- [7] A. H. Safavi-Naeini, J. Chan, J. T. Hill, T. P. Mayer Alegre, A. Krause, and O. Painter, Observation of Quantum Motion of a Nanomechanical Resonator, *Phys. Rev. Lett.* **108**, 033602 (2012).
- [8] D. Lee, M. Underwood, D. Mason, A. B. Shkarin, K. Börkje, S. M. Girvin, and J. G. E. Harris, [arXiv:1406.7254](https://arxiv.org/abs/1406.7254).
- [9] T. P. Purdy, R. W. Peterson, and C. A. Regal, Observation of radiation pressure shot noise on a macroscopic object, *Science* **339**, 801 (2013).
- [10] D. W. C. Brooks, T. Botter, S. Schreppler, T. P. Purdy, N. Brahms, and D. M. Stamper-Kurn, Non-classical light generated by quantum-noise-driven cavity optomechanics, *Nature (London)* **488**, 476 (2012).
- [11] A. H. Safavi-Naeini, S. Gröblacher, J. T. Hill, J. Chan, M. Aspelmeyer, and O. Painter, Squeezed light from a silicon micromechanical resonator, *Nature (London)* **500**, 185 (2013).
- [12] T. P. Purdy, P.-L. Yu, R. W. Peterson, N. S. Kampel, and C. A. Regal, Strong Optomechanical Squeezing of Light, *Phys. Rev. X* **3**, 031012 (2013).
- [13] V. B. Braginsky and F. Y. Khalili, *Quantum Measurements* (Cambridge University Press, Cambridge, England, 1995).
- [14] H. J. Kimble, The quantum internet, *Nature (London)* **453**, 1023 (2008).
- [15] T. A. Palomaki, J. W. Harlow, J. D. Teufel, R. W. Simmonds, and K. W. Lehnert, Coherent state transfer between itinerant microwave fields and a mechanical oscillator, *Nature (London)* **495**, 210 (2013).
- [16] R. W. Andrews, R. W. Peterson, T. P. Purdy, K. Cicak, R. W. Simmonds, C. A. Regal, and K. W. Lehnert, Bidirectional and efficient conversion between microwave and optical light, *Nat. Phys.* **10**, 321 (2014).
- [17] M. Bagheri, M. Poot, M. Li, W. P. H. Pernice, and H. X. Tang, Dynamic manipulation of nanomechanical resonators in the high-amplitude regime and non-volatile mechanical memory operation, *Nat. Nanotechnol.* **6**, 726 (2011).
- [18] M. Poggio and C. L. Degen, Force-detected nuclear magnetic resonance: Recent advances and future challenges, *Nanotechnology* **21**, 342001 (2010).
- [19] LIGO Scientific Collaboration, A gravitational wave observatory operating beyond the quantum shot-noise limit, *Nat. Phys.* **7**, 962 (2011).
- [20] LIGO Scientific Collaboration, Enhanced sensitivity of the LIGO gravitational wave detector by using squeezed states of light, *Nat. Photonics* **7**, 613 (2013).
- [21] A. Pontin, C. Biancofiore, E. Serra, A. Borrielli, F. S. Cataliotti, F. Marino, G. A. Prodi, M. Bonaldi, F. Marin, and D. Vitali, Frequency-noise cancellation in optomechanical systems for ponderomotive squeezing, *Phys. Rev. A* **89**, 033810 (2014).
- [22] A. Pontin, M. Bonaldi, A. Borrielli, F. S. Cataliotti, F. Marino, G. A. Prodi, E. Serra, and F. Marin, Squeezing a Thermal Mechanical Oscillator by Stabilized Parametric Effect on the Optical Spring, *Phys. Rev. Lett.* **112**, 023601 (2014).
- [23] A. Pontin, M. Bonaldi, A. Borrielli, F. S. Cataliotti, F. Marino, G. A. Prodi, E. Serra, and F. Marin, Detection of weak stochastic forces in a parametrically stabilized micro-optomechanical system, *Phys. Rev. A* **89**, 023848 (2014).
- [24] E. Serra, F. S. Cataliotti, F. Marin, F. Marino, A. Pontin, G. A. Prodi, and M. Bonaldi, Inhomogeneous mechanical losses in micro-oscillators with high reflectivity coating, *J. Appl. Phys.* **111**, 113109 (2012).
- [25] E. Serra, A. Borrielli, F. S. Cataliotti, F. Marin, F. Marino, A. Pontin, G. A. Prodi, and M. Bonaldi, A “low-deformation mirror” micro-oscillator with ultra-low optical and mechanical losses, *Appl. Phys. Lett.* **101**, 071101 (2012).
- [26] C. Fabre, M. Pinard, S. Bourzeix, A. Heidmann, E. Giacobino, and S. Reynaud, Quantum-noise reduction using a cavity with a movable mirror, *Phys. Rev. A* **49**, 1337 (1994).
- [27] S. Mancini and P. Tombesi, Quantum noise reduction by radiation pressure, *Phys. Rev. A* **49**, 4055 (1994).
- [28] D. Z. Anderson, J. C. Frisch, and C. S. Masser, Mirror reflectometer based on optical cavity decay time, *Appl. Opt.* **23**, 1238 (1984).
- [29] H. Davies, The reflection of electromagnetic waves from a rough surface, *Proc. IEE* **101**, 209 (1954).
- [30] F. Marino, F. S. Cataliotti, A. Farsi, M. S. de Cumis, and F. Marin, Classical Signature of Ponderomotive Squeezing in a Suspended Mirror Resonator, *Phys. Rev. Lett.* **104**, 073601 (2010).
- [31] F. Marino and F. Marin, Thermo-optical nonlinearities and stability conditions for high-finesse interferometers, *Phys. Lett. A* **364**, 441 (2007).
- [32] F. Marino and F. Marin, Coexisting attractors and chaotic canard explosions in a slow-fast optomechanical system, *Phys. Rev. E* **87**, 052906 (2013).

- [33] L. Conti, M. De Rosa, and F. Marin, Low-amplitude-noise laser for AURIGA detector optical readout, *Appl. Opt.* **39**, 5732 (2000).
- [34] L. Mandel, Sub-Poissonian photon statistics in resonance fluorescence, *Opt. Lett.* **4**, 205 (1979).
- [35] C. J. Hood, H. J. Kimble, and J. Ye, Characterization of high-finesse mirrors: Loss, phase shifts, and mode structure in an optical cavity, *Phys. Rev. A* **64**, 033804 (2001).
- [36] S. Joshi, S. Hung, and S. Vengallatore, Design strategies for controlling damping in micromechanical and nanomechanical resonators, *Eur. Phys. J. Tech. Instrum.* **1**, 5 (2014).
- [37] D. Kleckner, W. Marshall, M. J. A. de Dood, K. N. Dinyari, B.-J. Pors, W. T. M. Irvine, and D. Bouwmeester, High Finesse Opto-Mechanical Cavity with a Movable Thirty-Micron-Size Mirror, *Phys. Rev. Lett.* **96**, 173901 (2006).
- [38] D. Kleckner, B. Pepper, E. Jeffrey, P. Sonin, S. M. Thon, and D. Bouwmeester, Optomechanical trampoline resonators, *Opt. Express* **19**, 19708 (2011).
- [39] F. A. Torres, P. Meng, L. Ju, C. Zhao, D. G. Blair, K.-Y. Liu, S. Chao, M. Martyniuk, I. Roch-Jeune, R. Flaminio, and C. Michel, High quality factor mg-scale silicon mechanical resonators for 3-mode optoacoustic parametric amplifiers, *J. Appl. Phys.* **114**, 014506 (2013).
- [40] A. G. Kuhn, J. Teissier, L. Neuhaus, S. Zerkanı, E. van Brackel, S. Deleglise, T. Briant, P.-F. Cohadon, A. Heidmann, C. Michel, L. Pinard, V. Dolique, R. Flaminio, R. Taıbi, C. Chartier, and O. Le Traon, Free-space cavity optomechanics in a cryogenic environment, *Appl. Phys. Lett.* **104**, 044102 (2014).
- [41] M. Imboden and P. Mohanty, Dissipation in nano-electromechanical systems, *Phys. Rep.* **534**, 89 (2014).
- [42] J. P. Zendri, M. Bignotto, M. Bonaldi, M. Cerdonio, L. Conti, L. Ferrario, N. Liguori, A. Maraner, E. Serra, and L. Taffarello, Loss budget of a setup for measuring mechanical dissipations of silicon wafers between 300 K and 4 K, *Rev. Sci. Instrum.* **79**, 033901 (2008).
- [43] K. Yamamoto, S. Miyoki, T. Uchiyama, H. Ishitsuka, M. Ohashi, and K. Kuroda, Measurement of the mechanical loss of a cooled reflective coating for gravitational wave detection, *Phys. Rev. D* **74**, 022002 (2006).
- [44] T. H. Metcalf and Xiao Liu, An ultra-high Q silicon compound cantilever resonator for Young's modulus measurements, *Rev. Sci. Instrum.* **84**, 075001 (2013).
- [45] A. Borrielli, M. Bonaldi, E. Serra, A. Bagolini, and L. Conti, Wideband mechanical response of a high-Q silicon double-paddle oscillator, *J. Micromech. Microeng.* **21**, 065019 (2011).
- [46] G. D. Cole, I. Wilson-Rae, K. Werbach, M. R. Vanner, and M. Aspelmeyer, Phonon-tunnelling dissipation in mechanical resonators, *Nat. Commun.* **2**, 231 (2011).
- [47] The effective mass is determined by the oscillating mass and by the coupling factor of the mode with the cavity length, and must be evaluated by FE simulation. However, in our device the resonator mode and the main mode of the outer filter induce an oscillation exactly along the axis of the cavity, therefore their effective mass is approximately equal to the physical mass. The torsional and rocking modes of the device usually have an effective mass much larger than their physical mass, as they are only weakly coupled to the cavity.
- [48] I. Tittonen, G. Breitenbach, T. Kalkberner, T. Müller, R. Conradt, and S. Schiller, Interferometric measurements of the position of a macroscopic body: Towards observation of quantum limits, *Phys. Rev. A* **59**, 1038 (1999).
- [49] E. Serra, A. Borrielli, F. S. Cataliotti, F. Marin, F. Marino, A. Pontin, G. A. Prodi, and M. Bonaldi, Ultralow-dissipation micro-oscillator for quantum optomechanics, *Phys. Rev. A* **86**, 051801(R) (2012).
- [50] A. Pontin, M. Bonaldi, A. Borrielli, F. Marino, L. Marconi, A. Bagolini, G. Pandraud, E. Serra, and F. Marin, Dynamical back-action effects in low loss optomechanical oscillators, *Ann. Phys. (Berlin)* **527**, 89 (2015).
- [51] A. Farsi, M. Siciliani de Cumis, F. Marino, and F. Marin, Photothermal and thermo-refractive effects in high reflectivity mirrors at room and cryogenic temperature, *J. Appl. Phys.* **111**, 043101 (2012).
- [52] T. Klitsner, J. E. VanCleve, H. E. Fischer, and R. O. Pohl, Phonon radiative heat transfer and surface scattering, *Phys. Rev. B* **38**, 7576 (1988).
- [53] E. Serra, A. Bagolini, A. Borrielli, M. Boscardin, F. S. Cataliotti, F. Marin, F. Marino, A. Pontin, G. A. Prodi, M. Vannoni, and M. Bonaldi, Fabrication of low loss MOMS resonators for quantum optics experiments, *J. Micromech. Microeng.* **23**, 085010 (2013).
- [54] The estimate is not accurate mainly because the devices have slightly different sizes and resonance frequencies.
- [55] J. D. Thompson, B. M. Zwickl, A. M. Jayich, F. Marquardt, S. M. Girvin, and J. G. E. Harris, Strong dispersive coupling of a high finesse cavity to micromechanical membrane, *Nature (London)* **452**, 72 (2008).
- [56] L. G. Villanueva and S. Schmid, Evidence of Surface Loss as Ubiquitous Limiting Damping Mechanism in SiN Micro- and Nanomechanical Resonators, *Phys. Rev. Lett.* **113**, 227201 (2014).
- [57] J. Qin, C. Zhao, Y. Ma, X. Chen, L. Ju, and D. G. Blair, Classical demonstration of frequency-dependent noise ellipse rotation using optomechanically induced transparency, *Phys. Rev. A* **89**, 041802(R) (2014).
- [58] Y. Tao, J. M. Boss, B. A. Moores, and C. L. Degen, Single-crystal diamond nanomechanical resonators with quality factors exceeding one million, *Nat. Commun.* **5**, 3638 (2014).
- [59] G. D. Cole, W. Zhang, M. J. Martin, J. Ye, and M. Aspelmeyer, Tenfold reduction of Brownian noise in high-reflectivity optical coatings, *Nat. Photonics* **7**, 644 (2013).